RESEARCH ARTICLE

Centrifugally spun poly(ethylene oxide) fibers rival the properties of electrospun fibers

Jorgo Merchiers[1,2] | Carina D. V. Martínez Narváez[3] | Cheryl Slykas[3] | Mieke Buntinx[1,2] | Wim Deferme[1,2] | Jan D'Haen[1,2] | Roos Peeters[1,2] | Vivek Sharma[3] | Naveen K. Reddy[1,2]

[1]Institute for Materials Research (IMO-IMOMEC), Hasselt University, Diepenbeek, Belgium

[2]IMEC vzw, Division IMOMEC, Diepenbeek, Belgium

[3]Department of Chemical Engineering, University of Illinois at Chicago, Chicago, Illinois, 60608, USA

Correspondence
Vivek Sharma, Department of Chemical Engineering, University of Illinois at Chicago, Chicago, IL, USA.
Email: viveks@uic.edu
Naveen K. Reddy, Institute for Materials research (IMO-IMOMEC), Hasselt University, B-3590 Diepenbeek, Belgium.
Email: naveen.reddy@uhasselt.be

Abstract

Centrifugal force spinning (CFS), also known as centrifugal spinning, forcespinning, or rotary jet spinning, provides considerably higher production rates than electrospinning (ES), but the more widespread use of CFS as an alternative depends on the ability to produce fibers with robust thermal and mechanical properties. Here, we report the CFS of poly(ethylene oxide) (PEO) fibers made using a spinning dope formulated with acetonitrile (AcN) as the volatile solvent, and we describe the thermal and mechanical properties of the centrifugally-spun fibers. Even though the formation, diameter, and morphology of electrospun and centrifugally-spun PEO fibers are relatively well-studied, the article presents three crucial contributions: the pioneering use of PEO solutions in AcN as spinning dope, characterization of crystallinity and mechanical properties of the centrifugally-spun PEO fibers, and a comparison with the corresponding properties of electrospun fibers. We find that fiber formation occurrs for the chosen CFS conditions if polymer concentration exceeds the entanglement concentration, determined from the measured specific viscosity. Most significantly, the centrifugally spun PEO fibers display crystallinity, modulus, elongation-at-break, and fiber diameter that rival the properties of electrospun PEO fibers reported in the literature.

KEYWORDS
centrifugal spinning, entangled polymers, fiber spinning, nonwovens, rheology, rotary jet spinning

1 | INTRODUCTION

Fundamental research in electrospinning (ES) and centrifugal force spinning (CFS) is driven by the technological need to produce fibers and nonwoven structures from specialized ingredients, or tackle application needs not addressed using conventional materials and spinning technologies.[1–6] Examples include high surface area, controlled mesh-like nonwoven structures for on-demand deployment in applications ranging from wound dressing and tissue engineering,[2,3,7–9] separation and filtration,[10,11] energy storage and production,[12,13] food processing,[14–16] and most recently, to create masks to prevent air-borne infections.[17] ES relies on electrostatic forces to draw a Taylor cone from a pendant droplet of a viscoelastic, polymeric liquid, and turn the cone into a liquid jet that undergoes drawing and thinning via whipping (and other) instabilities.[3,5–8,18–21] In contrast, in

CFS, a spiraling liquid jet ejected from a fast rotating spinneret or nozzle under the influence of centrifugal forces, undergoes drawing and thinning during its time-of-flight, t_{flight} to a collector.[2,3,6–8,22–32] In both cases, the final draw ratio and the fiber diameter additionally depend on the crystallization and solidification processes that transform a liquid (solution or melt) jet to a solid filament over a timescale t_{jf} that needs to be shorter than t_{flight}. CFS has been reinvented many times since its inception with various names like centrifugal spinning, forcespinning, cotton candy method, rotary jet spinning and rotary spinning,[2,3,6–8,13,22–33] to make cotton candy, fiberglass, microfibers, polymeric fibers from solutions and melts, and composite fibers. Extensive experimental and theoretical studies of ES have explored the influence of polymer, solvent, and other additives (particles, cells, surfactants, and drugs), processing conditions, and post-spinning operations like annealing on spinnability, fiber morphology and mechanical properties.[6–8,19,20,34–36] However, after three decades of ES research, the practical need for a high voltage source, low production rate, and limited range of spinnable formulations continue to drive the search for faster, cheaper, safer alternatives.

Among the alternatives, we picked CFS as our technique of choice as it offers relatively high production rates with a comparatively simple set-up that does not require a specialized environment, high voltage, or specialized material (conductivity) properties.[2–4,21–25,31] Several reviews and research articles discuss the relative merits of both ES and CFS, and though many studies highlight the higher production rate as a distinct advantage of centrifugal force spinning,[2–4,12,23–25,31–33] comparisons of crystallinity and mechanical properties of fibers and fiber mats are nearly nonexistent. We noticed only two studies[37,38] used differential scanning calorimetry (DSC) to obtain crystallinity for nylon and regenerated silk and found comparable values for electrospun and centrifugally-spun fibers. As ES and CFS differ vastly in terms of the driving forces that can stretch and align polymers,[6,20,25–27,39] determine timescales for solidification, growth of capillarity-driven instability, and the time-of-flight from nozzle to collector,[7,8] it is critical to contrast diameter, crystallinity, and mechanical properties of centrifugally-spun fibers with electrospun fibers. In practical applications, mechanical properties of fibers and consequently fiber mats (nonwovens) affect perceived stiffness or softness, bending and folding resistance, toughness, and the impact and flexural strength of any materials formed with them.[1,21,35] The feasibility and utility for use as wearable and smart textiles, filtration, biomaterials (e.g., for wound dressing and tissue engineering), and energy storage of nonwoven materials are

dependent on their mechanical properties.[3,7,8,16,40–42] Crystallinity influences mechanical properties as well as chemical resistance, sorption behavior, density, and dyeing behavior.[1] Even though nearly all studies characterize fiber diameter, and many discuss the influence of solvent type and polymer properties on spinnability and fiber morphology,[7,8,31] very few centrifugal spinning papers characterize and contrast the crystallinity and mechanical properties, motivating this study.

In this contribution, we identify the concentration range for which solutions of poly(ethylene oxide) (PEO) in acetonitrile (AcN) form beads-on-a-string and continuous filaments on centrifugal force spinning (CFS) with a home-built set-up[43] using matched processing parameters like rotational speed, nozzle diameter, and the nozzle-collector distance. We examine the concentration-dependent variation in steady shear viscosity of the spinning dope via torsional rheometry, and we characterize the thermal and mechanical properties of the centrifugally spun fiber mats. We contrast crystallinity, tensile strength and modulus, and elongation-at-break with the corresponding values reported in literature for electrospun PEO fibers. We picked PEO as the model polymer inspired by many existing fundamental studies of fiber formation and properties,[2,4,8,12,13,18,21,24,27,29,33,34,40,44–49] and our extensive prior characterization of the shear and extensional rheology response of aqueous PEO solutions.[50–53] Fibers formed by PEO alone, using PEO to enhance spinnability, or containing PEO blended with other polymers, particles, or proteins, are suitable for biomedical (e.g., drug delivery, antimicrobial filters), energy and digital electronics (e.g., battery separators, photovoltaics), and environmental applications.[7,8,12,13,40,42,48,49,54] We anticipate that the analysis of thermal and mechanical properties of centrifugally-spun fibers will spur critical progress toward a better understanding of processing-structure–property relationships, needed for designing application-specific nonwovens.

2 | MATERIALS AND METHODS

PEO of molecular weight, $M_w = 600$ kg/mol (Sigma-Aldrich) was dissolved in AcN solvent (HPLC grade, VWR chemicals) under mild mixing conditions to minimize chain scission and to ensure homogeneous mixing. We used a home-built centrifugal spinning set-up to spin fibers for a range of PEO concentrations with matched processing parameters like rotational speed (4000 rpm), temperature (298 K), distance to the collector (12 cm), and nozzle diameter (0.6 mm). The bespoke set-up is

designed to allow use of different nozzles and includes lifting and shifting mechanisms to allow exquisite control over nozzle-collector distance. The design specifications and considerations for the set-up, and the influence of nozzle properties and rotational speed are detailed in a previous contribution.[43] The SEM images were acquired using a ZEISS Gemini 450 (Zeiss, Zaventem, Belgium). The diameter and standard deviation in size were analyzed in ImageJ. The steady shear viscosity was characterized using an ARG2 stress-controlled rheometer (TA Instruments, New Castle, DE, USA), with cone-and-plate geometry (40 mm diameter, 1° cone angle) at 25°C. The temperature was maintained using a Peltier element, and we used a solvent trap to minimize the influence of solvent evaporation on the measurements. The DSC measurements were carried out on a Q200 instrument (TA Instruments, Asse, Belgium). The temperature was varied between 20 and 150°C, at a heating/cooling rate of 20°C/min. The tensile testing was carried out on centrifugally-spun fiber mats (60 mm × 10 mm) using a Tinius Olsen (5ST) apparatus (Redhill, UK), with a tensile speed of 10 mm/min, and preload of 0.2 N.

3 | RESULTS AND DISCUSSION

The centrifugal spinning of PEO/AcN solutions results in fibers for polymer concentration, $c > 2$ wt.%, whereas the solutions with $c < 2$ wt.% produced only a spray of droplets. Fiber size and morphology were visualized and analyzed using images obtained via scanning electron microscopy (SEM), as shown in Figure 1. Beaded fibers or beads-on-a-string filamentous structures form at low concentrations (2–3 wt.%), and continuous fibers form at the highest three concentrations shown (4–6 wt.%). However, centrifugal forces generated by the chosen processing parameters produce relatively low stress to propel continuous jets for polymer concentration beyond 6 wt.%. Thus, the spinnability range of PEO/AcN solutions for centrifugal fiber spinning at 4000 rpm lies between 2 and 6 wt.%, in agreement with
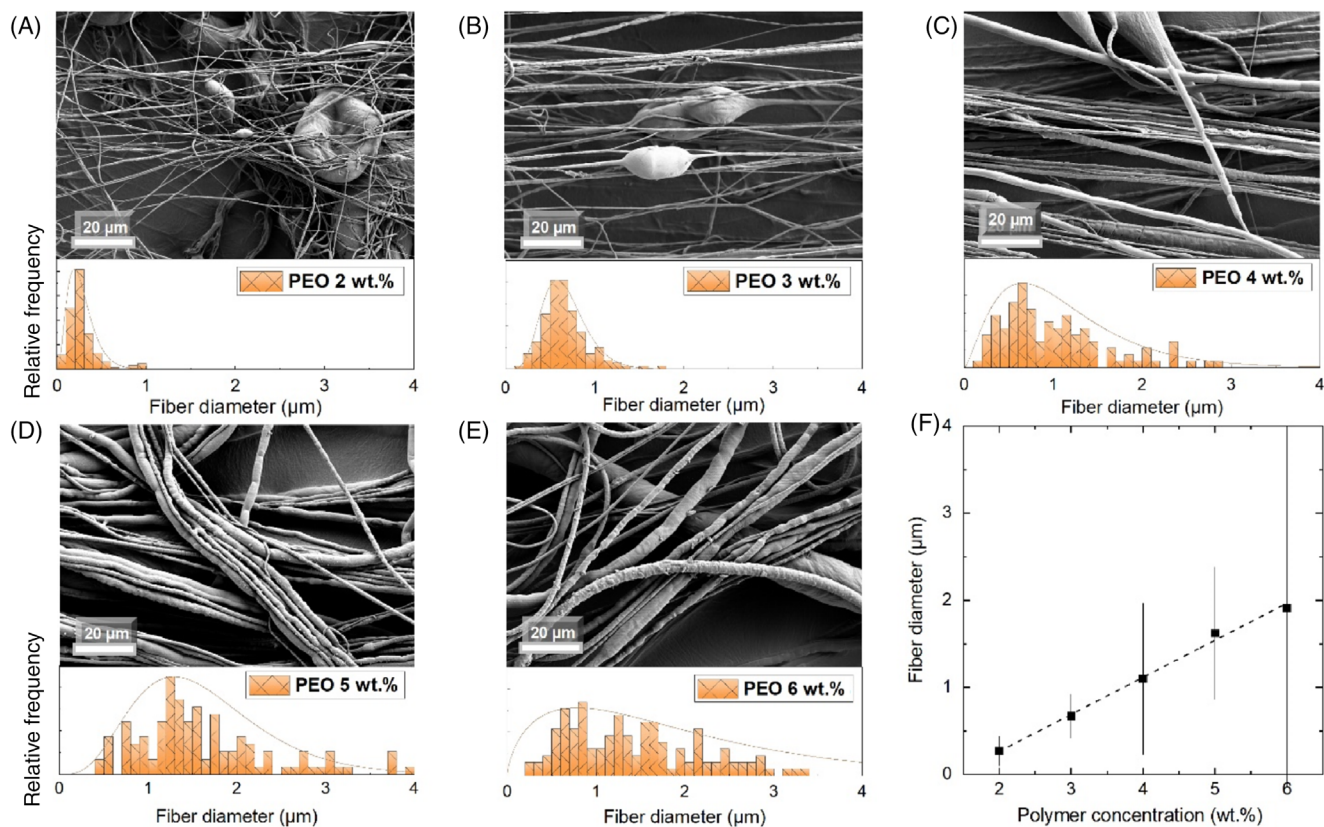
FIGURE 1 Diameter and morphology of the centrifugally-spun PEO fibers. (A,B) beads form, and fiber diameter size distribution is relatively narrow. (C–E) increase in PEO concentration leads to a rise in diameter, formation of continuous fibers, and broader size distribution. The scale bar corresponds to 20 μm. The diameter and standard deviation in size were analyzed in ImageJ. (F) Fiber diameter increases linearly with polymer concentration. The PEO fibers are centrifugally spun under matched processing conditions (4000 rpm and nozzle size = 0.6 mm) using AcN as the volatile solvent

the previous reports (based on other solvents).[55,56] Figure 1F shows that the average diameter of fibers centrifugally-spun under matched conditions increases with polymer concentration. The average fiber diameter was determined by averaging over at least 100 measured values, each obtained using the ImageJ software, by analyzing at least three SEM images for each concentration.

As the change in morphology from drops to beaded and continuous fibers is primarily governed by the role played by the rheological response, we characterized the shear rheology response using torsional rheometry. Steady shear viscosity as a function of shear rate, $\dot{\gamma}$, is plotted in FIGURE 2A for PEO solutions formulated with pure AcN as a solvent. The white region in the plot identifies the measurable range, whereas the gray zones represent regimes inaccessible due to the low torque limit (left) and the secondary flow limit (right).[57] The steady shear viscosity appears to be rate-independent for concentrations below 2 wt.%. However, PEO solutions for $c > 2$ wt.% show a Newtonian plateau at a low shear rate followed by a pronounced shear thinning regime. We used solvent viscosity, η_s and zero-shear viscosity, η_0, to compute the specific viscosity, $\eta_{sp} = (\eta_0 - \eta_s)/\eta_s$. The plot of η_{sp} as a function of the polymer concentration included as Figure 2B shows that all solutions are nondilute, as $\eta_{sp} > 1$, and η_{sp} values lie in two distinct regimes that display $\eta_{sp} \propto c^k$, with $k = 1.7$ and $k = 4.6$, respectively. The scaling exponents can be compared with $k = 2$ and $k = 4.7$, respectively observed for semi-dilute unentangled and entangled aqueous PEO solutions.[58]

The change from unentangled to entangled behavior in Figure 2B occurs at the entanglement concentration, $c_e \approx 1.8$ wt.%. In qualitative agreement with many previous studies,[7,8,59–61] PEO solutions in AcN appear to form continuous fibers under matched spinning conditions for $c > c_e$. The increase in polymer concentration in the entangled regime results in a substantial increase in the shear viscosity of the spinning dope (see Figure 2). Furthermore, the onset of shear thinning regimes shifts to lower shear rates, consistent with increase in elasticity and shear relaxation time. Additionally, entangled solutions of flexible polymers like PEO display a concentration-dependent increase in the relaxation modulus, normal stress differences, and extensional viscosity.[6,46,50–52,57,58,60] The concentration-dependent changes in viscosity and viscoelasticity impact the onset and growth of surface tension-driven instabilities that drive sinusoidal perturbations of cylindrical jets,[62–64] and lead to the formation of (spray) drops and beads-on-a-string structures observed here for the unentangled PEO solutions (Table 1).[7,8]

Next, we describe the thermal properties of the fibers as characterized using DSC. Figure 3A shows the first heating curves obtained for the as-spun fibers, whereas the first cooling curves acquired after erasing the thermal and processing history by heating up to 150°C are shown in Figure 3B. A second heating curve was recorded as a reference for visualizing the changes in thermal properties after erasing the microstructure of the fibrous material. The numbers in Figure 3A denote the melting temperature, T_m, the crystallization temperature, T_c, and the heat of crystalline melting, ΔH_m, determined by integration of the area under the melting peak, (as shown for the bulk sample). The crystallinity, X_c, of the samples is calculated using $X_c = \frac{\Delta H_m}{\Delta H_m^*} \times 100\%$, where the melting enthalpy for pure crystalline PEO, $\Delta H_m^* = 213.7$ J/g. The heating curves show an apparent increase in melting enthalpy, while the melting peak, T_m, remains roughly the same for all samples around 66 to 67 °C. Thus, the computed crystalline
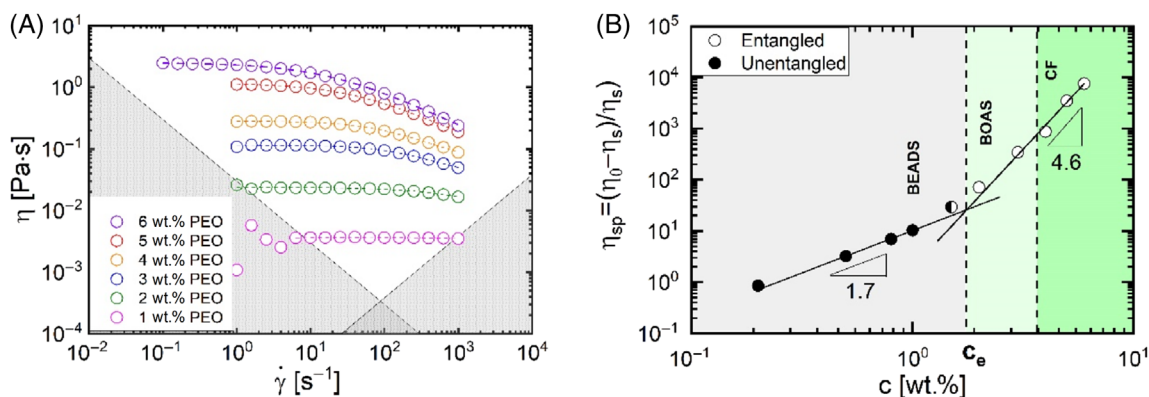
FIGURE 2 Shear rheology response of the PEO solutions formulated in pure AcN as a solvent. (A) Steady shear viscosity as a function of shear rate displays a concentration-dependent increase. PEO solution with $c > 1$ wt.% exhibit shear thinning. (B) Specific shear viscosity as a function of concentration displays two distinct regimes corresponding to unentangled and entangled semi-dilute solutions, respectively. The shaded regions correspond to beads (or drops), BOAS (beads-on-a-string), and CF (continuous fibers) morphology, respectively

TABLE 1 Experimentally determined values of the zero-shear viscosity (η_0) of PEO solutions, the calculated specific viscosity (η_{sp}), the fiber diameter (Φ) and its standard deviation, and the fiber morphology characterized in terms of a presence or an absence of beads in the fiber mat.

c [wt.%]	η_0 [pa·s]	η_{sp}	Φ [μm]	Bead formation
2	0.024	71	0.27 ± 0.17	Yes
3	0.12	343	0.67 ± 0.25	Yes
4	0.28	874	1.10 ± 0.87	No
5	1.17	3468	1.62 ± 0.76	No
6	2.51	7447	1.91 ± 2.04	No
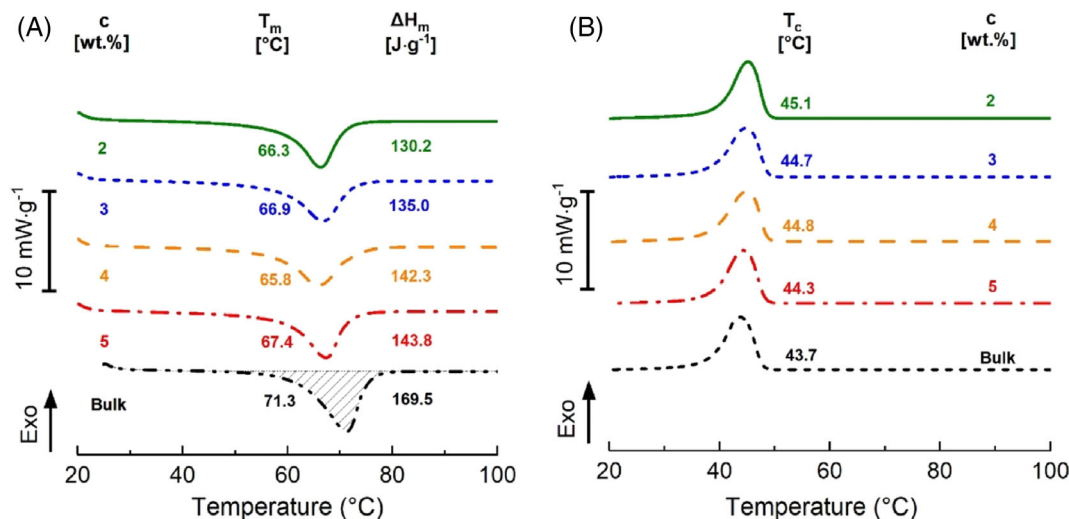
FIGURE 3 DSC thermograms of the spun fiber mats. (A) The heating curves show the influence of difference in crystallinity and melting peak for the fibers spun from different concentrations of PEO in AcN. A bulk PEO sample (powder) is included for comparison. (B) The cooling curves for the same samples show crystallization peak is nearly matched. The temperature was varied between 20 and 150°C, at a heating/cooling rate of 20°C/min

TABLE 2 Comparison of thermal properties of PEO fiber mats obtained using centrifugal fiber spinning (this work, with AcN as solvent) contrasted with the reported properties of PEO fiber mats obtained using ES formed using the listed solvents.

Φ (μm)	T_m (°C)	ΔH_m (J/g)	X_c (%)	T_c (°C)	ΔH_c (J/g)	Method/Reference	Solvent
0.27	66.3	130.2	61	45.1	112	CFS	AcN
0.67	66.9	135.0	64	44.7	114	CFS	AcN
1.10	65.8	142.3	66	44.8	110	CFS	AcN
1.62	67.4	143.8	67	44.3	113	CFS	AcN
0.50	64	83	44	46	-	ES[65]	CHCl$_3$
0.20–0.25	≈65–70	-	-	-	-	ES[66]	H$_2$O
0.24	67	165	84	45	169	ES[40]	CHCl$_3$
0.45	66	175	73	39	-	ES[41]	H$_2$O
2.00	68	-	-	-	-	ES[67]	H$_2$O
0.14	72	141.4	66	-	-	ES[68]	H$_2$O
0.70–2.70	65		74			ES[69]	H$_2$O & DMF
-	66	146	53	40		ES[56]	H$_2$O

fraction in the fibers increases with an increase in the polymer concentration from $X_c = 60.9\%$ for fibers spun from a 2 wt.% solution to much higher $X_c = 67.3\%$, for the fibers spun from a 5 wt. % solution. The overall crystallinity of the fibers is lower than the value of $X_c = 79.3\%$ obtained for the same bulk polymer.

A comparison of the cooling curves included in Figure 3B shows that the crystallization peak, T_c, arises within a small range of temperatures 44.3 to 45.1°C, and the values are in the same range as that of the bulk material. We compared the thermal properties of centrifugally-spun fibers to those reported in the literature for electrospun PEO fibers and listed the values in Table 2. Even though polymer molecular weight, solvent, polymer concentration in spinning dope, and processing condition are significantly different, the overall crystallinity, enthalpy of melting, and melting point compare relatively well with the electrospun fibers. As comparable crystalline fraction and macromolecular orientation could lead to similar mechanical properties for semicrystalline polymeric fibers, we characterized the mechanical properties and contrasted them with those of electrospun fibers.

The analysis of stress–strain data provides a quantitative measurement of tensile strength and elongation-at-break, whereas the area under the curve provides a measure of toughness, as shown in Figure 4A. Furthermore, Young's modulus is extracted from the slope of the linear response at low applied strain (Figure 4B). The yield point is not observed for any of the fibrous samples. It is well-established that once an individual fiber starts softening, surrounding fibers in the mat bear a higher load, leading to a smooth increase in stress instead of a sharp peak observed in the mechanical response of the bulk material. The mechanical properties extracted from the analysis of stress–strain data are included in Figure 4 and are listed in Table 3. Young's modulus, tensile strength, and toughness increase with fiber diameter, and the results correlate well with a similar rise in crystallinity manifested in the thermal properties.

Surprisingly few reports include any data for thermal or mechanical properties of centrifugally-spun fibers, and almost none compare the mechanical properties to electrospun fibers. To the best of our knowledge, Table 3 presents the only such comparison. We find that Young's modulus values of centrifugally spun fibers ($\sim$5–15 MPa), extracted from the slope of stress–strain curve as shown in Figure 4B, are in the same range as the values reported for electrospun fiber mats.[16,42] However, our centrifugally-spun fiber mats show higher values for the tensile strength (fibers from CFS: 1.8–4.2 MPa, compared to fibers from ES: 0.2–2.4 MPa) and elongation-at-break
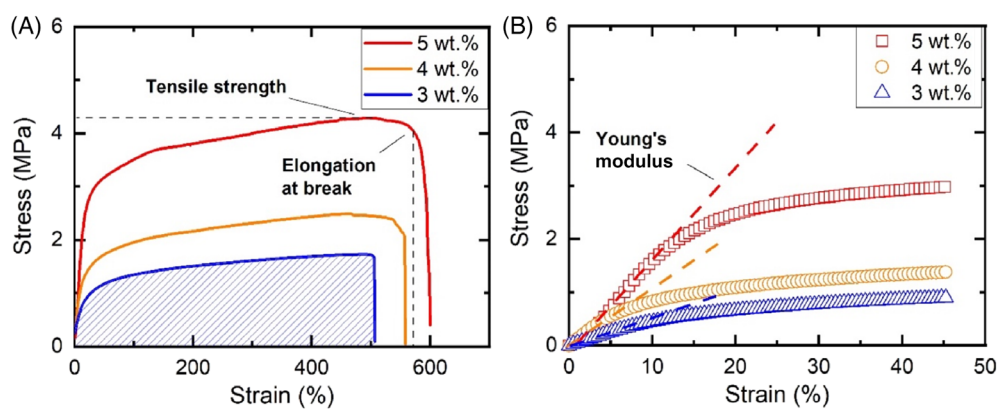
FIGURE 4 Mechanical properties of centrifugally spun PEO fiber mats. (A) Stress–strain curves shown for fibers spun from three concentrations, and tensile strength and elongation-at-break are highlighted. (B) Stress–strain curves are shown in the small strain limit to highlight concentration-dependent variation in Young's modulus

TABLE 3 Mechanical properties of centrifugally spun PEO fiber mats (this work) contrasted with those reported for electrospun PEO fibers in literature. An aqueous solution with 2% acetic acid (AA) (v/v) was used in the final reference.

Mw (kg/mol)	Φ (nm)	Tensile strength (MPa)	Young's modulus (MPa)	Elongation at break (−)	Toughness (kJ·m⁻³)	Method/ Reference	Solvent
600	670	1.80 ± 0.72	4.88 ± 0.72	445.9 ± 62.5	695 ± 95	CFS	AcN
600	1100	2.49 ± 0.15	8.21 ± 1.66	628.5 ± 43.5	1348 ± 131	CFS	AcN
600	1620	4.23 ± 0.76	15.3 ± 2.14	517.5 ± 78.2	1897 ± 499	CFS	AcN
100	240	0.20 ± 0.03	4 ± 2	15 ± 4	-	ES[40]	CHCl$_3$
1000	446	1.60 ± 0.16	20 ± 1	152 ± 31	-	ES[41]	H$_2$O
900	300–2000	≈ 1.25	-	-	-	ES[42]	H$_2$O
900	227	2.40 ± 0.56	-	68 ± 2	-	ES[16]	AA in H$_2$O

(and are, therefore, likely to show higher toughness). We have characterized the mechanical properties of centrifugally spun PEO fiber mats produced using other solvents, including AcN-water mixtures, and found mechanical properties are comparable to the values included in Table 3. Even though a more extensive study of fiber properties is needed (and underway), the trends show centrifugal spun fibers can rival the mechanical properties and crystallinity of electrospun fibers.

Even though there are many studies that use PEO alone or as an additive for ES,[21,28,40–42,54,66,67] only a countable few describe mechanical properties.[16,35,40–42] Table 3 includes mechanical properties of electrospun PEO fiber mats, along with the data for the fiber diameters, the choice of solvent, and the polymer molecular weight. The processing parameters are not included in the table for brevity's sake, even though they can exercise an influence on fiber diameter and morphology. The diameters of centrifugally spun PEO fibers in this study (see Tables 2 and 3) are larger than the diameters of electrospun fibers. Even though fiber diameters and mechanical properties can be changed by altering polymer (M_w, polydispersity in M_w, and polymer concentration) or processing conditions (for CFS, by changing RPM, nozzle diameter and the nozzle-collector distance), we present these as-measured values to emphasize that centrifugal force spinning, even with modest processing conditions, facilitates a high throughput production of PEO fibers with crystallinity and mechanical properties comparable to electrospun fibers.

4 | CONCLUSIONS

In summary, we determined that the spinnable solutions of PEO in AcN are in entangled regime by examining the concentration-dependent variation in steady shear viscosity of the spinning dope measured via torsional rheometry. We find that the centrifugal spinning of PEO in AcN leads to fiber formation for entangled solutions (above 2 wt.% for PEO with M_w = 600 kg/mol). Under matched processing conditions (4000 rpm, and nozzle diameter = 0.6 mm), the diameter of the centrifugally-spun fibers increases linearly with polymer concentration. The thermal characterization carried out using DSC shows that crystallinity values, and the tensile testing data show that Young's modulus and tensile strength values of the centrifugally spun PEO fibers are in the same range as for electrospun PEO fibers. However, the elongation-at-break is considerably higher for centrifugally spun fibers. We anticipate that the comparison and compilation of crystallinity and mechanical properties presented herein will provide a significant impetus for

the research and application of centrifugal force spinning. Additionally, we show that PEO fibers can be produced by using AcN as a nonaqueous solvent, and this presents opportunities for spinning PEO fibers blended with molecules, particles, proteins, or polymers that have specific functionality, but low or poor solubility in water.

The comparisons (included in Tables 2 and 3) are presented with the understanding that the absolute values measured are influenced by variability in the orientation of individual filaments, the difference in fiber diameter, rheological properties of the spinning dopes and processing conditions, choice of polymer and solvent. Fascinatingly, a recent review on mechanical properties of electrospun fibers by Rashid, Gorga, and Krause[35] summarizes the innumerable challenges involved in contrasting mechanical properties even for fibers electrospun with matched materials and processing conditions. The various challenges include a lack of standardized testing methods and protocols, difficulties involved in characterizing properties of single fibers and fiber mats, and the impact of fiber orientation, diameter, surface roughness on properties of fiber mats.[35] Notwithstanding these challenges, the significance of the comparison between the representative values for centrifugally-spun and electrospun PEO fibers is in presenting the necessary first step toward a deeper understanding of connections between rheology, processing, structure and properties, and designing nonwovens well-suited for varied application areas. We anticipate that the evidence for strikingly similar mechanical properties, in addition to faster production rates, will enhance the interest, research and capital investment in utilizing CFS for making nonwoven structures with semi-crystalline polymers for the applications affected by crystallinity, strength, modulus and elongation-at-break.

that have contributed to the ideas in this paper (some 20-plus years later!).

DATA AVAILABILITY STATEMENT
The raw data is available, on request, from the corresponding authors.

ORCID
Jorgo Merchiers https://orcid.org/0000-0003-3909-9004
Carina D. V. Martínez Narváez https://orcid.org/0000-0002-2356-7208
Cheryl Slykas https://orcid.org/0000-0002-7189-8490
Mieke Buntinx https://orcid.org/0000-0002-4249-0779
Wim Deferme https://orcid.org/0000-0002-8982-959X
Roos Peeters https://orcid.org/0000-0001-7515-802X
Vivek Sharma https://orcid.org/0000-0003-1152-1285
Naveen K. Reddy https://orcid.org/0000-0002-4919-2977

REFERENCES
[1] V. B. Gupta, V. K. Kothari Eds., *Manufactured Fiber Technology*, Chapman & Hall, London **1997**.
[2] B. Atıcı, C. H. Ünlü, M. Yanilmaz, *Polym. Rev* **2021**, 1. https://doi.org/10.1080/15583724.2021.1901115
[3] D. M. Dos Santos, D. S. Correa, E. S. Medeiros, J. E. Oliveira, L. H. C. Mattoso, *ACS Appl. Mater. Interfaces* **2020**, *12*, 45673.
[4] A. Barhoum, K. Pal, H. Rahier, H. Uludag, I. S. Kim, M. Bechelany, *Appl. Mater. Today* **2019**, *17*, 1.
[5] E. Ewaldz, B. Brettmann, *ACS Appl. Polym. Mater.* **2019**, *1*, 298.
[6] J. H. Park, G. C. Rutledge, *Macromolecules* **2017**, *50*, 5627.
[7] J. Venugopal, S. Ramakrishna, *Appl. Biochem. Biotechnol.* **2005**, *125*, 147.
[8] Q. P. Pham, U. Sharma, A. G. Mikos, *Tissue Eng.* **2006**, *12*, 1197.
[9] K. A. Rieger, N. P. Birch, J. D. Schiffman, J. Mater, *Chem. B* **2013**, *1*, 4531.
[10] K. Yoon, B. S. Hsiao, B. Chu, *J. Mater. Chem.* **2008**, *18*, 5326.
[11] F. E. Ahmed, B. S. Lalia, R. Hashaikeh, *Desalination* **2015**, *356*, 15.
[12] B. Ding, J. Yu, *Electrospun Nanofibers for Energy and Environmental Applications*, New York: Springer, **2014**.
[13] R. O. Chavez, T. P. Lodge, M. Alcoutlabi, *Mater. Sci. Eng., B* **2021**, *266*, 115024.
[14] I. Kutzli, M. Gibis, S. K. Baier, J. Weiss, *Food Hydrocolloids* **2019**, *93*, 206.
[15] B. Ghorani, N. Tucker, *Food Hydrocolloids* **2015**, *51*, 227.
[16] D. Surendhiran, C. Li, H. Cui, L. Lin, *Food Packag. Shelf Life* **2020**, *23*, 100439.
[17] M. M. Bandi, *Proc. R. Soc. A* **2020**, *476*, 20200469.
[18] J. Doshi, D. H. Reneker, *J. Electrostatics* **1995**, *35*, 151.
[19] D. H. Reneker, A. L. Yarin, *Polymer* **2008**, *49*, 2387.
[20] M. M. Hohman, M. Shin, G. Rutledge, M. P. Brenner, *Phys. Fluids* **2001**, *13*, 2221.
[21] M. Richard-Lacroix, C. Pellerin, *Macromolecules* **2013**, *46*, 9473.
[22] R. T. Weitz, L. Harnau, S. Rauschenbach, M. Burghard, K. Kern, *Nano Lett.* **2008**, *8*, 1187.
[23] K. Sarkar, C. Gomez, S. Zambrano, M. Ramirez, E. de Hoyos, H. Vasquez, K. Lozano, *Mater. Today* **2010**, *13*, 12.
[24] M. R. Badrossamay, H. A. McIlwee, J. A. Goss, K. K. Parker, *Nano Lett.* **2010**, *10*, 2257.
[25] S. Padron, A. Fuentes, D. Caruntu, K. Lozano, *J. Appl. Phys.* **2013**, *113*, 024318.
[26] S. Noroozi, H. Alamdari, W. Arne, R. G. Larson, S. M. Taghavi, *J. Fluid Mech.* **2017**, *822*, 202.
[27] S. Noroozi, W. Arne, R. G. Larson, S. M. Taghavi, *J. Fluid Mech.* **2020**, *892*, A26-1.
[28] L. Ren, R. Ozisik, S. P. Kotha, P. T. Underhill, *Macromolecules* **2015**, *48*, 2593.
[29] Y. Fang, A. D. Dulaney, J. Gadley, J. M. Maia, C. J. Ellison, *Polymer* **2015**, *73*, 42.
[30] Y. Fang, A. R. Dulaney, J. Gadley, J. Maia, C. J. Ellison, *Polymer* **2016**, *88*, 102.
[31] J. J. Rogalski, C. W. Bastiaansen, T. Peijs, *NANO* **2017**, *3*, 97.
[32] H. Xu, H. Chen, X. Li, C. Liu, B. Yang, *J. Polym. Sci. Part B: Polym. Phys* **2014**, *52*, 1547.
[33] X. Zhang, Y. Lu, *Polym. Rev.* **2014**, *54*, 677.
[34] R. Jaeger, M. M. Bergshoef, C. M. I. Batlle, H. Schönherr, G. Julius Vancso, *Macromol. Symp.* **1998**, *127*, 141.
[35] T. U. Rashid, R. E. Gorga, W. E. Krause, *Adv. Eng. Mater* **2021**, 1. https://doi.org/10.1002/adem.202100153
[36] L. Palangetic, N. K. Reddy, S. Srinivasan, R. E. Cohen, G. H. McKinley, C. Clasen, *Polymer* **2014**, *55*, 4920.
[37] J. J. Rogalski, C. W. M. Bastiaansen, T. Peijs, *Fibers* **2018**, *6*, 37.
[38] C. Liu, J. Sun, M. Shao, B. Yang, *RSC Adv.* **2015**, *5*, 98553.
[39] A. L. Yarin, S. Koombhongse, D. H. Reneker, *J. Appl. Phys.* **2001**, *89*, 3018.
[40] A. Bianco, M. Calderone, I. Cacciotti, *Mater. Sci. Eng. C* **2013**, *33*, 1067.
[41] X. Xu, H. Wang, L. Jiang, X. Wang, S. A. Payne, J. Y. Zhu, R. Li, *Macromolecules* **2014**, *47*, 3409.
[42] Y. A. Samad, A. Asghar, R. Hashaikeh, *Renewable Energy* **2013**, *56*, 90.
[43] J. Merchiers, W. Meurs, W. Deferme, R. Peeters, M. Buntinx, N. K. Reddy, *Polymer* **2020**, *12*, 575.
[44] S. Padron, R. Patlan, J. Gutierrez, N. Santos, T. Eubanks, K. Lozano, *J. Appl. Polym. Sci.* **2012**, *125*, 3610.
[45] S. Mahalingam, M. Edirisinghe, *Macromol. Rapid Commun.* **2013**, *34*, 1134.
[46] J. H. Yu, S. V. Fridrikh, G. C. Rutledge, *Polymer* **2006**, *47*, 4789.
[47] M. E. Helgeson, K. N. Grammatikos, J. M. Deitzel, N. J. Wagner, *Polymer* **2008**, *49*, 2924.

[48] M. T. Hasan, R. Gonzalez, M. Chipara, L. Materon, J. Parsons, M. Alcoutlabi, *Polym. Adv. Technol.* **2021**, *32*, 2327.

[49] S. T. Sullivan, C. Tang, A. Kennedy, S. Talwar, S. A. Khan, *Food Hydrocolloids* **2014**, *35*, 36.

[50] J. Dinic, M. Biagioli, V. Sharma, *J. Polym. Sci. Part B: Polym. Phys* **2017**, *55*, 1692.

[51] J. Dinic, Y. Zhang, L. N. Jimenez, V. Sharma, *ACS Macro Lett.* **2015**, *4*, 804.

[52] J. Dinic, V. Sharma, *Proc. Natl. Acad. Sci. U. S. A.* **2019**, *116*, 8766.

[53] C. D. V. Martínez Narváez, T. Mazur, V. Sharma, *Soft Matter* **2021**, *17*, 6116.

[54] X. Li, Y. Lu, T. Hou, J. Zhou, B. Yang, *Micro Nano Lett.* **2018**, *13*, 1688.

[55] Z. Zhiming, S. Jun, D. Yaoshuai, L. Binbin, *J. Brazilian Soc. Mech. Sci. Eng.* **2018**, *40*, 1.

[56] C. Li, Y. Huang, R. Li, Y. Wang, X. Xiang, C. Zhang, D. Wang, Y. Zhou, X. Liu, W. Xu, *Carbohydr. Polym.* **2021**, *251*, 117037.

[57] C. W. Macosko, *Rheology: Principles, Measurements and Applications*, New York: VCH Publishers, Inc., **1994**.

[58] M. Rubinstein, R. H. Colby, *Polymer Physics*, Oxford Univ. Press, New York **2003**.

[59] S. L. Shenoy, W. D. Bates, H. L. Frisch, G. E. Wnek, *Polymer* **2005**, *46*, 3372.

[60] P. Gupta, C. Elkins, T. E. Long, G. L. Wilkes, *Polymer* **2005**, *46*, 4799.

[61] S. J. Haward, V. Sharma, C. P. Butts, G. H. McKinley, S. S. Rahatekar, *Biomacromolecules* **2012**, *13*, 1688.

[62] V. Sharma, S. J. Haward, J. Serdy, B. Keshavarz, A. Soderlund, P. Threlfall-Holmes, G. H. McKinley, *Soft Matter* **2015**, *11*, 3251.

[63] A. L. Yarin, *Free Liquid Jets and Films: Hydrodynamics and Rheology*, Harlow: Longman Scientific & Technical, **1993**.

[64] J. Eggers, *Rev. Mod. Phys.* **1997**, *69*, 865.

[65] G.-M. Kim, A. Wutzler, H.-J. Radusch, G. H. Michler, P. Simon, R. A. Sperling, W. J. Parak, *Chem. Mater.* **2005**, *17*, 4949.

[66] A. Aluigi, A. Varesano, A. Montarsolo, C. Vineis, F. Ferrero, G. Mazzuchetti, C. Tonin, *J. Appl. Polym. Sci.* **2007**, *104*, 863.

[67] Z. Li, S. Mei, Y. Dong, F. She, L. Kong, *Polymer* **2019**, *11*, 1550.

[68] K. Škrlec, Š. Zupančič, S. P. Mihevc, P. Kocbek, J. Kristl, A. Berlec, *Eur. J. Pharm. Biopharm.* **2019**, *136*, 108.

[69] A. W. Laramee, C. Lanthier, C. Pellerin, *ACS Appl. Polym. Mater.* **2020**, *2*, 5025.